Inorganic Chemistry Communications 177 (2025) 114300

Contents lists available at ScienceDirect

Inorganic Chemistry Communications

journal homepage: www.elsevier.com/locate/inoche

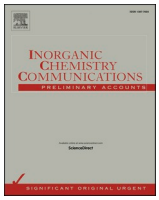

Short communication

Modulation of optoelectronic properties of WO_3 thin film via Cr doping through RF co-sputtering

Md. Mahfuzul Haque [a,b,c,*], Samiya Mahjabin [a,d], Md. Ariful Islam [a,c,e], Vidhya Selvanathan [f], Yoganash Putthisigamany [a], Huda Binti Abdullah [g], Faiz Arith [h], Md. Akhtaruzzaman [i], Mohd Adib Ibrahim [a], Puvaneswaran Chelvanathan [a,**]

[a] Solar Energy Research Institute, Universiti Kebangsaan Malaysia, 43600 Bangi, Selangor, Malaysia
[b] Department of Mathematical and Physical Sciences, Faculty of Sciences and Engineering, East West University, Dhaka 1212, Bangladesh
[c] Institute of Advanced Research and Technology (IART), Dhaka Solar Ltd., Dhaka 1212, Bangladesh
[d] Department of Physics, American International University-Bangladesh, Kuratoli, Dhaka 1229, Bangladesh
[e] Centre for Advanced Research in Sciences, University of Dhaka, Bangladesh
[f] Institute of Sustainable Energy, Universiti Tenaga Nasional, Malaysia
[g] Department of Electrical, Electronic and Systems Engineering, Universiti Kebangsaan Malaysia, 43600 Bangi, Selangor, Malaysia
[h] Faculty of Electronics and Computer Technology and Engineering, Universiti Teknikal Malaysia Melaka, Malaysia
[i] Department of Chemical Engineering, Faculty of Engineering, Islamic University of Madinah, 42351 Madinah, Saudi Arabia

ARTICLE INFO

Keywords:
Cr-doped WO_3
Perovskite solar cells
RF sputtering
Thin film
Electron transport layer

ABSTRACT

Tungsten trioxide (WO_3) has drawn significant interest for its diverse applications, including electrochromic devices, perovskite solar cells, and gas sensors among others, due to its tunable properties. This study investigates the impact of chromium (Cr) doping on WO_3 thin films deposited via RF co-sputtering. X-ray diffraction and Raman spectroscopy confirmed Cr incorporation, enhancing crystallinity. UV–Vis spectroscopy verified the improvement in transmittance and revealed an increase in the energy bandgap with Cr doping. Field emission scanning electron microscopy revealed reduced grain size and increased surface roughness with higher Cr doping. Additionally, electrical measurements indicated decreased conductivity. The enhanced transmittance and widened energy bandgap suggest that Cr-doped WO_3 could serve as an efficient electron transport layer in n-i-p structured perovskite solar cells. These findings demonstrate that controlled Cr doping effectively tailors WO_3 properties, providing valuable insights for optimizing its performance in optoelectronic applications.

1. Introduction

Tungsten trioxide (WO_3), a well-studied transition metal oxide, has gained significant attention for its versatile applications, including electrochromic devices, photocatalysis, gas sensors, smart windows, and photovoltaics, due to its versatile properties. Particularly, WO_3 is increasingly gaining attention as a promising electron transport layer (ETL) in perovskite solar cells (PSCs) [1,2]. Additionally, high chemical and thermal stability have made WO_3 ceramics crucial in various functional ceramics. To utilize WO_3 in diverse applications, its properties have been extensively optimized through doping with various elements. For example, silver (Ag) doping enhances the gas-sensing performance of WO_3 [3], whereas zinc (Zn) doping boosts its photo electrocatalytic efficiency [4,5] and gadolinium (Gd) doping enhances the electrochromic properties of WO_3 [6,7]. In the research field of PSCs, europium (Eu) doping improves WO_3's functionality as charge transport layers [8], while niobium (Nb) doping enhances electron transport by increasing donor density and minimizing trap states, though it also reduces transmittance [9]. Molybdenum (Mo) doping further improves the electron transporting properties of WO_3 and significantly enhances the stability of PSCs, but it decreases the transmittance [10]. Similarly, Ag doping reduces the bandgap, thereby reducing the visible-light transmittance [11]. While the effects of Cr doping on WO_3 have not been widely studied, existing reports suggest that it induces significant structural modifications, which may influence its optical and electrical behavior. Given its potential impact on multiple material properties, further

* Corresponding author at: Solar Energy Research Institute, Universiti Kebangsaan Malaysia, 43600 Bangi, Selangor, Malaysia.
** Corresponding author.
E-mail addresses: mahfuz.ap@gmail.com (Md. Mahfuzul Haque), cpuvaneswaran@ukm.edu.my (P. Chelvanathan).

https://doi.org/10.1016/j.inoche.2025.114300
Received 4 January 2025; Received in revised form 23 February 2025; Accepted 6 March 2025
Available online 9 March 2025
1387-7003/© 2025 Elsevier B.V. All rights are reserved, including those for text and data mining, AI training, and similar technologies.

investigation is essential to understand its suitability for optoelectronic and sensing applications.

Although various techniques, such as flame spray pyrolysis [12], hydrothermal [13], and liquid–liquid doping precursor [14], were used to deposit Cr-doped WO_3, to the best of our knowledge, it has not yet been deposited through radio frequency (RF) sputtering technique, that offers several advantages, such as precise control over film composition, thickness, and uniform deposition [15]. RF sputtering is an industrially viable and scalable technique, making it suitable for large-area deposition while ensuring high reproducibility [16]. Although this method may involve higher initial setup costs compared to certain chemical synthesis methods, it provides improved target utilization, lower contamination risk, and minimized material waste, all of which contribute to enhanced long-term cost efficiency [16,17]. Moreover, as a vacuum-based process, RF sputtering eliminates the need for hazardous chemical precursors, making it a more environmentally friendly and sustainable method for large-scale Cr-doped WO_3 film production.

In this study, we deposited Cr-doped WO_3 through RF co-sputtering and investigated doping effects on the material's structure, morphology, and optical and electrical properties. By comparing Cr doping with other dopants, this work contextualizes its unique advantages within the broader field of doped WO_3 materials and provides insights into its potential applications.

2. Methodology

Undoped WO_3 was sputtered by using the sputtering machine (Model 4G-3RF-1DC, Kurt J. Lesker) at room temperature for 45 min under Ar gas flow of 6 sccm, providing RF power of 100 W at WO_3 target (99.9% purity, 2″ diameter, Kurt J. Lesker). Cr-doped WO_3 films were sputtered by applying 8 W and 20 W co-sputtering powers at Cr target (99.9% purity, 2″ diameter, Kurt J. Lesker), while keeping all other parameters unchanged. All films were annealed under vacuum at 550 °C for 40 min. Optical transmittance and absorbance were measured using a Perkin Elmer Lambda 950 UV–Vis–NIR spectrophotometer. Structural analysis was conducted via a Bruker AXS-D8 X-ray diffractometer with Cu Kα radiation (λ = 1.5406 Å). Raman spectroscopy was performed with a Thermo Scientific DXR2xi confocal micro-Raman imaging microscope, utilizing a 532 nm laser excitation wavelength, 5 mW power, and a 1 μm spot size. Surface morphology and elemental composition were analyzed using a ZEISS MERLIN FESEM with EDX.

3. Results and discussion

X-ray diffraction patterns for undoped and Cr-doped WO_3 thin films (Fig. 1(a)) match with the standard XRD spectrum of orthorhombic WO_3 (PDF Card No. 00-020-1234). As the co-sputtering power increases, a slight peak shift towards lower angles occurs because W^{6+} (ionic radius 0.60 Å) are substituted by larger Cr^{3+} (0.615 Å), expanding the lattice and increasing the d-spacing [13]. Moreover, narrower and more intense peaks are observed in Cr-doped films compared to undoped film, with more pronounced peaks at higher co-sputtering power. The inset of Fig. 1(a) highlights the shifting, narrowing and increased intensity of the dominant peak (200). Crystallite sizes (L) for this peak were calculated by using Scherrer's equation ($L = 0.9\lambda/\beta\cos\theta$, where β represents the full width at half maximum (FWHM) of the peak at the angle 2θ) and found to be 8.57 nm (undoped), 9.48 nm (8 W Cr-doped), and 10.73 nm (20 W Cr-doped), indicating enhanced crystallinity with increased Cr doping, further supported by the rise in peak intensity. A shoulder peak at approximately 23.50° near the (200) plane of the undoped WO_3 film is observed, which can be attributed to secondary phases or minor structural distortions inherent in the undoped RF-sputtered WO_3. This auxiliary peak diminishes with the introduction and incremental doping of Cr, likely due to the stabilization of the orthorhombic phase through the minimization of distortions or secondary phases, thereby enhancing crystallinity.

In the Raman spectra (Fig. 1(b)), the ~270 cm^{-1} peak corresponds to O–W–O bending vibration, while the ~700 cm^{-1} and ~808 cm^{-1} peaks indicate O–W–O stretching modes [13,18]. These vibrational modes are caused by the periodic movement of atoms inside the lattice; stretching modes include the expansion and contraction of bond lengths, whilst bending modes involve angular deformations of the O–W–O bond. The inset of Fig. 1(b) shows the ~808 cm^{-1} peak shifting toward lower wavenumbers (redshift) as co-sputtering power increases. In Raman spectroscopy, a redshift occurs when a vibrational mode moves to a lower frequency, typically indicating a weakening of the corresponding bond. This shift suggests lengthened O–W–O bonds, which can be attributed to the incorporation of Cr ions into the WO_3 lattice. This incorporation induces bond lengthening and lattice expansion, consistent with the XRD analysis. Moreover, a prominent peak ~995 cm^{-1} appears with the increment of co-sputtering power, whereas it is absent in undoped WO_3. This peak represents a new vibrational mode and is commonly associated with the Cr=O stretching mode, suggesting that Cr incorporation into the WO_3 lattice modifies the local bonding environment. The formation of Cr=O bonds likely results from Cr ions occupying substitutional or interstitial sites within the WO_3 framework, influencing vibrational modes and local symmetry. Previous studies have linked this peak to terminal Cr=O bonds, which are characteristic of chromium oxides or Cr-doped oxide systems [13]. The intensity increase of the ~995 cm^{-1} peak with higher Cr doping further supports the presence of more Cr=O bonds, indicating progressive Cr incorporation into the WO_3 lattice. This structural alteration can impact the material's electronic and optical properties, which is crucial for its application in optoelectronic devices.

The transmittance spectra for both undoped and doped films (Fig. 2 (a)) indicate increased transparency upon Cr doping, with further

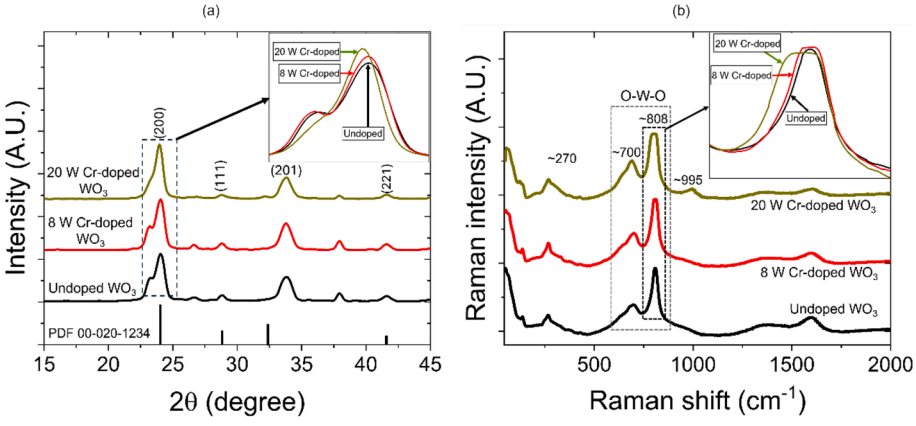

Fig. 1. A) XRD pattern and b) Raman spectra of undoped, 8 W Cr-doped and 20 W Cr-doped WO_3 films.

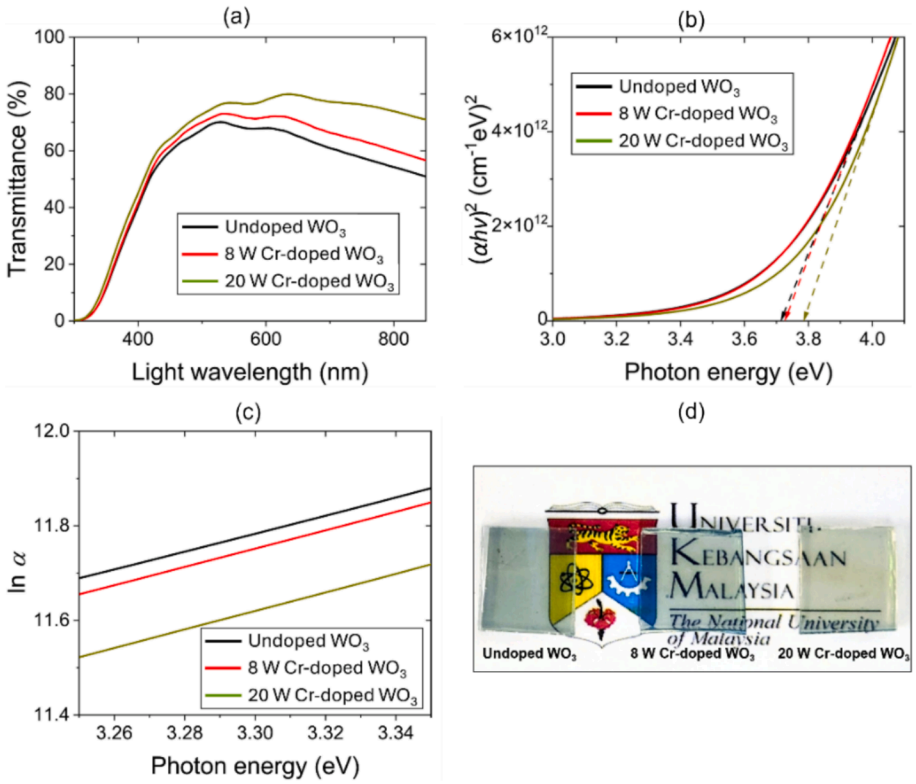

Fig. 2. (a) Transmittance spectra, (b) Tauc plot, (c) ln α vs $h\nu$ plot, (d) visible transparency of the films.

enhancement at higher co-sputtering powers. The undoped film shows an average transmittance of ~60%, while 8 W and 20 W Cr-doped films exhibit transmittances of ~65% and ~75%, respectively. This increment may be attributed to the gradual improvement of crystallinity and increased crystallite size. Larger crystallites generally lead to fewer defects that scatter light, resulting in higher optical transmittance. Additionally, the enhanced transmittance is likely linked to the gradual disappearance of the auxiliary peak around 23.50° in the XRD pattern, indicating a secondary phase. The improved transmittance of the ETL is particularly beneficial for n-i-p structured PSCs, as it facilitates greater light penetration into the perovskite absorber layer, enhancing light absorption and photocurrent generation. Consequently, Cr doping in WO_3 improves its functionality as an ETL, potentially leading to improved solar cell efficiency.

The absorption coefficient (α) is crucial for determining the optical energy bandgap (E_g) and the Urbach energy (E_U) of thin films. The values of α were determined for all films from absorbance (A) and thickness (d) of the films by using the relation: $\alpha = 2.303$ (A/d) [19,20]. To determine E_g using the Tauc method, $(\alpha h\nu)^2$ versus photon energy ($h\nu$) was plotted for each film, as shown in Fig. 2(b). By extrapolating the linear region of these graphs to the $h\nu$-axis, the intersection points represent the E_g values. This analysis reveals that Cr doping gradually increases the E_g values. For undoped WO_3, the E_g is 3.72 eV, increasing to 3.73 eV and 3.78 eV for 8 W and 20 W Cr-doped films, respectively, indicating a blue shift with Cr doping. The determined E_g values fall within the range reported in the literature [10,21–23]. This increase in E_g may be attributed to the Burstein-Moss effect, where Cr incorporation raises the Fermi level by additional electrons, filling lower conduction band states. Thus the electrons are required to be excited only to higher energy states above the Fermi level, effectively increasing the apparent E_g [24,25]. As an ETL with a higher E_g absorbs less visible light than one with a lower E_g, more photons can reach the perovskite absorber layer, enhancing photon absorption and charge generation in n-i-p-structured PSCs. Cr-doped WO_3 proves beneficial n-i-p structured PSCs by enabling better utilization of photons with energies below its bandgap but above that of the perovskite. This enhanced light-harvesting improves short-circuit current and overall solar cell performance.

Urbach energy (E_U) provides information regarding the disorders in materials such as thermal, structural and compositional disorders. It is related to α and $h\nu$ by the relation: $\ln \alpha = \ln \alpha_0 + h\nu/E_U$ [22]. ln α vs $h\nu$ was plotted for all the films to determine the E_U. In the lower energy region of these plots, where α increases exponentially as $h\nu$ approaches E_g, the most linear segments are identified which are shown in Fig. 2(c). By inverting the slopes of these linear parts, the E_U values are determined as 524.41 meV, 514.4 meV, and 509.02 meV for undoped, 8 W and 20 W Cr-doped WO_3 films, respectively. Fig. 2(d) demonstrates the visible transparency of the films, showing that visibility through the films increases with the level of Cr doping.

FESEM images of all films (Fig. 3) show that undoped film has larger particles than doped films. As Cr-doping is introduced and increased, the average particle size decreases gradually from ~220 nm (undoped) to ~180 nm (20 W Cr-doped), enhancing densification. Cr doping likely breaks larger particles into smaller ones, increasing grain boundaries and surface area. Less distinct grain boundaries and greater granularity are observed in the doped films as particles begin to overlap for higher co-sputtering power, indicating an increase in roughness, making the 20 W Cr-doped film the roughest. Elemental analysis shows that Cr is undetected in 8 W Cr-doped WO_3 film, likely due to its content being below the machine's detection limit but detected in 20 W Cr-doped film.

Under dark condition, the current density (mA/cm^2) vs. voltage (V) was measured for the sputtered films of 1 cm^2 area on FTO using an LIV measurement device with direct electrical connections (without using any top contact) to the FTO and the thin film, ensuring that the observed conductivity originates from the WO_3 layer. The current density vs voltage graph in Fig. 3(d) shows that undoped WO_3 has the highest slope, reflecting the highest conductivity. Cracks in this film, found from the FESEM images may lead to the electrical shorting, contributing to this conductivity. In contrast, Cr-doped WO_3 films exhibit decreasing slopes with increased co-sputtering power, indicating reduced conductivity. This reduction may be due to the defect states or scattering

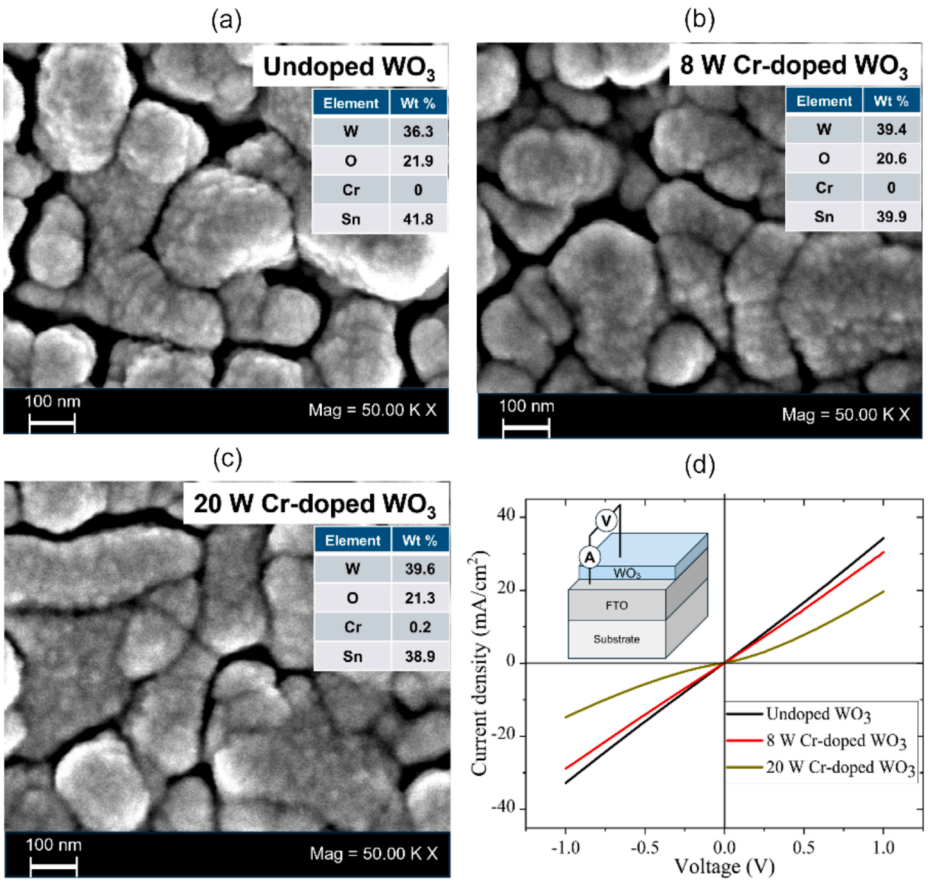

Fig. 3. Surface morphology and elemental composition of (a) undoped, (b) 8 W and (c) 20 W Cr-doped WO_3 film, (d) I-V characteristics of all films.

centers introduced by Cr doping, acting as traps or recombination sites, which hamper charge carrier mobility. Furthermore, Cr ions may occupy interstitial positions or substitute W sites, introducing lattice distortions that increase charge carrier scattering, as evidenced by the XRD data showing lattice expansion. The higher grain boundary density, as observed in FESEM images, further impedes charge transport by increasing grain boundary scattering. At higher doping levels, ionized impurity scattering also hinders the carrier movement. Together, these factors create barriers to charge transport, leading to the observed decrease in conductivity with increased Cr doping.

4. Conclusion

Post-annealed RF sputtered WO_3 films exhibited an orthorhombic phase, as confirmed by XRD analysis, with Cr doping leading to increased phase purity. Cr doping reduced the crystallite size from 8.57 nm (undoped) to 10.73 nm (20 W Cr-doped), contributing to improved crystallinity. This enhancement in crystallinity resulted in a significant increase in the average transmittance of the films, from ~60% (undoped) to ~75% (20 W Cr-doped). Furthermore, Cr doping slightly increased the energy bandgap from 3.72 eV (undoped) to 3.73 eV (8 W Cr-doped) and further to 3.78 eV (20 W Cr-doped film), indicating a proportional relationship between Cr concentration and the energy bandgap. Observed peak shifting in XRD analysis of Cr-doped films toward lower angle, indicating lattice expansion and formation of a new vibrational mode at 995 cm^{-1} in Raman spectroscopy of Cr-doped films, attributed to Cr=O stretching, confirmed the replacement of W ions by Cr ions. Compared to other dopants, Cr doping offers unique advantages for ETL applications in perovskite solar cells (PSCs). While Ag doping reduces the bandgap and lowers visible-light transmission, Mo doping enhances ETL properties and improves PSC stability but decreases transmittance. Similarly, Nb doping improves electron transport; however, it also reduces transmittance, which can limit light absorption in the perovskite layer. In contrast, Cr doping simultaneously enhances crystallinity and maintains high transparency, ensuring efficient photon transmission. Its moderate bandgap increase benefits n-i-p PSCs by minimizing ETL absorption, allowing more light to reach the perovskite layer and improving charge generation. Unlike Mo and Nb doping, Cr doping strikes a balance among structural enhancement, optical performance, and bandgap modulation, making it a promising choice for high-transparency ETLs with efficient charge transport and optimized light management in PSCs. These findings demonstrate that well-controlled Cr doping via RF co-sputtering effectively tailors the properties of WO_3 films, making them highly attractive for energy-efficient and optoelectronic applications.

CRediT authorship contribution statement

Md. Mahfuzul Haque: Writing – original draft, Methodology, Investigation, Data curation, Conceptualization. **Samiya Mahjabin:** Writing – review & editing, Visualization, Formal analysis. **Md. Ariful Islam:** Visualization, Software. **Vidhya Selvanathan:** Writing – review & editing, Methodology. **Yoganash Putthisigamany:** Visualization, Investigation. **Huda Binti Abdullah:** Project administration, Funding acquisition. **Faiz Arith:** Validation, Formal analysis. **Md. Akhtaruzzaman:** Formal analysis, Writing – review & editing. **Mohd Adib Ibrahim:** Supervision, Resources. **Puvaneswaran Chelvanathan:** Writing – review & editing, Supervision, Methodology, Formal analysis, Conceptualization.

Declaration of competing interest

The authors declare that they have no known competing financial interests or personal relationships that could have appeared to influence the work reported in this paper.

Acknowledgement

We acknowledge the Universiti Kebangsaan Malaysia, Malaysia for financial support through DIP-2021-013 research grant.

Data availability

No data was used for the research described in the article.

References

[1] M.M. Haque, S. Mahjabin, H.B. Abdullah, Md. Akhtaruzzaman, H. Almohamadi, M. A. Islam, M.I. Hossain, M.A. Ibrahim, P. Chelvanathan, Exploring the theoretical potential of tungsten oxide (WOx) as a universal electron transport layer (ETL) for various perovskite solar cells through interfacial energy band alignment modulation, *J. Phys. Chem. Solid*, 196 (2025) 112324, https://doi.org/10.1016/J.JPCS.2024.112324.

[2] S. Mahjabin, et al., Perceiving of defect tolerance in perovskite absorber layer for efficient perovskite solar cell, *IEEE Access* 8 (July) (2020) 106346–106353, https://doi.org/10.1109/ACCESS.2020.3000217.

[3] C. Bittencourt, et al., Ag induced modifications on WO3 films studied by AFM, Raman and x-ray photoelectron spectroscopy, *J. Phys. D Appl. Phys.* 37 (24) (Dec. 2004) 3383, https://doi.org/10.1088/0022-3727/37/24/005.

[4] X.F. Cheng, W.H. Leng, D.P. Liu, J.Q. Zhang, C.N. Cao, Enhanced photoelectrocatalytic performance of Zn-doped WO3 photocatalysts for nitrite ions degradation under visible light, *Chemosphere* 68 (10) (Aug. 2007) 1976–1984, https://doi.org/10.1016/J.CHEMOSPHERE.2007.02.010.

[5] M. Arshad, et al., Synthesis and characterization of Zn doped WO3 nanoparticles: photocatalytic, antifungal and antibacterial activities evaluation, *Mater. Res. Express* 7 (1) (Jan. 2020) 015407, https://doi.org/10.1088/2053-1591/AB6380.

[6] Y. Yin, et al., Electrochromic and energy storage bifunctional Gd-doped WO3/Ag/WO3 films, *J. Mater. Chem. A* 8 (21) (Jun. 2020) 10973–10982, https://doi.org/10.1039/D0TA02079F.

[7] Y. Yin, C. Lan, S. Hu, C. Li, Effect of Gd-doping on electrochromic properties of sputter deposited WO3 films, *J. Alloy. Compd.* 739 (Mar. 2018) 623–631, https://doi.org/10.1016/j.jallcom.2017.12.290.

[8] X. Chen, et al., Europium ions doped WOx nanorods for dual interfacial modification facilitating high efficiency and stability of perovskite solar cells, *Nano Energy* 80 (Feb. 2021) 105564, https://doi.org/10.1016/J.NANOEN.2020.105564.

[9] K. Wang, et al., W(Nb)Ox-based efficient flexible perovskite solar cells: From material optimization to working principle, *Nano Energy* 31 (Jan. 2017) 424–431, https://doi.org/10.1016/j.nanoen.2016.11.054.

[10] S. Mahjabin, et al., Boosting perovskite solar cell stability through a sputtered Mo-doped tungsten oxide (WOx) electron transport layer, *Energy Fuel* 37 (24) (Dec. 2023) 19860–19869, https://doi.org/10.1021/ACS.ENERGYFUELS.3C03126/SUPPL_FILE/EF3C03126_SI_001.PDF.

[11] S. Mohammed Harshulkhan, K. Janaki, G. Velraj, R. Sakthi Ganapathy, S. Krishnaraj, Structural and optical properties of Ag doped tungsten oxide (WO3) by microwave-assisted chemical route, *J. Mater. Sci. Mater. Electron.* 27 (4) (2016) 3158–3163, https://doi.org/10.1007/S10854-015-4138-1.

[12] L. Wang, A. Teleki, S.E. Pratsinis, P.I. Gouma, Ferroelectric WO3 nanoparticles for acetone selective detection, *Chem. Mater.* 20 (15) (Aug. 2008) 4794–4796, https://doi.org/10.1021/CM800761E/SUPPL_FILE/CM800761E-FILE002.PDF.

[13] Q. Ding *et al.*, Cr-doped urchin-like WO3 hollow spheres: the cooperative modulation of crystal growth and energy-band structure for high-sensitive acetone detection, *Sensors* 20(12) (*2020*) 3473, doi: 10.3390/S20123473.

[14] X. Guozuan, R. Liu, Y. Qiumin, Y. Chenghui, H. Guohui, X. Xiang, Preparation and characterization of Cr-doped tungsten oxide by liquid-liquid doping precursor, *Mater. Res. Express* 8 (1) (Jan. 2021) 016509, https://doi.org/10.1088/2053-1591/ABD5CF.

[15] C. Fu, C. Yang, L. Han, H. Chen, The thickness uniformity of films deposited by magnetron sputtering with rotation and revolution, *Surf. Coatings Technol.* 200 (12–13) (Mar. 2006) 3687–3689, https://doi.org/10.1016/J.SURFCOAT.2004.12.023.

[16] H. Ghazal, N. Sohail, H. Ghazal, N. Sohail, Sputtering deposition, *Thin Film. - Depos. Methods Appl.* (Oct. 2022), https://doi.org/10.5772/INTECHOPEN.107353.

[17] D.K. Maurya, A. Sardarinejad, K. Alameh, Recent developments in R.F. magnetron sputtered thin films for ph sensing applications—an overview, Coatings 4 (4) (2014) 756–771, https://doi.org/10.3390/COATINGS4040756.

[18] C. Santato, M. Odziemkowski, M. Ulmann, J. Augustynski, Crystallographically oriented mesoporous WO3 films: synthesis, characterization, and applications, *J. Am. Chem. Soc.*, 123 (43) (Oct. 2001) 10639–10649, https://doi.org/10.1021/JA011315X.

[19] S. Ahmed, et al., Rf sputtered GZO thin films for enhancing electron transport in perovskite solar cells, *Opt. Mater.* 149 (2024) 115006, https://doi.org/10.1016/J.OPTMAT.2024.115006.

[20] S. Mahjabin, et al., Sputtered WOx thin film as the electron transport layer for efficient perovskite solar cells, *Appl. Phys. A Mater. Sci. Process.*, 128 (4) (Apr. 2022) 1–11, https://doi.org/10.1007/s00339-022-05500-5.

[21] S. Mahjabin, et al., Effects of oxygen concentration variation on the structural and optical properties of reactive sputtered WOx thin film, *Sol. Energy* 222 (May) (Jul. 2021) 202–211, https://doi.org/10.1016/j.solener.2021.05.031.

[22] S. Mahjabin, et al., Investigation of morphological, optical, and dielectric properties of RF sputtered WOx thin films for optoelectronic applications, *Nanomaterials* 12 (19) (Oct. 2022) 3467, https://doi.org/10.3390/NANO12193467/S1.

[23] A. Subrahmanyam, A. Karuppasamy, Optical and electrochromic properties of oxygen sputtered tungsten oxide (WO3) thin films, *Sol. Energy Mater. Sol. Cells* 91 (4) (Feb. 2007) 266–274.

[24] S. Gahlawat, J. Singh, A.K. Yadav, P.P. Ingole, Exploring Burstein–Moss type effects in nickel doped hematite dendrite nanostructures for enhanced photo-electrochemical water splitting, *PCCP*, 21 (36) (Sep. 2019) 20463–20477, https://doi.org/10.1039/C9CP04132J.

[25] Q. Zhu, J. Lu, Y. Wang, F. Qin, Z. Shi, C. Xu, Burstein-moss effect behind Au surface plasmon enhanced intrinsic emission of ZnO microdisks, Sci. Reports 6 (1) (2016) 1–9, https://doi.org/10.1038/srep36194.